

Direct Field and Mixed Potential Integral Equation Solutions by Fast Fourier Transform Accelerated Multilevel Green's Function Interpolation for Conducting and Impedance Boundary Objects

Dennis T. Schobert and Thomas F. Eibert

Lehrstuhl für Hochfrequenztechnik
Technische Universität München
Arcisstr. 21, 80333 München, Munich, Germany
schobert@ieee.org

Abstract — A fast solver based on multilevel Lagrange interpolation of homogenous space electric and magnetic field Green's functions is discussed. Broadband applications are possible due to a wavelength adaptive multilevel scheme. By an FFT-technique, the pertinent translation operators are diagonalized. An impedance boundary condition (IBC) is employed considering electric and magnetic currents for the approximate treatment of non-metallic objects. The common mixed-potential integral equation and a direct field formulation are both discussed. In general, the direct field formulation leads to more accurate results in conjunction with interpolated Green's functions, especially for low frequency problems. The efficiency of the algorithm is shown in several numerical examples.

Index Terms — Electromagnetic radiation, electromagnetic scattering, fast integral solvers, integral equations.

I. INTRODUCTION

Surface integral equation methods belong to the most efficient techniques for solving electromagnetic scattering or radiation problems. When employing method of moments (MoM) discretization, the integral equation (IE) operators are converted into matrix vector products [1, 2]. Unfortunately, these IE operators are in general fully populated, causing bad numerical complexities. This makes the computation of problems with many unknowns very challenging. Hierarchical fast solvers have been introduced to overcome this problem. One of the most popular methods is the multilevel fast multipole method (MLFMM) [2]. In this method, discretization elements with small separations are grouped hierarchically and far-

range interactions are computed among groups of basis functions on appropriate levels in the accordant hierarchy. Interactions between the single basis/testing functions are just contained in the translation operators between elements, which are very close to each other. Due to the strongly increasing magnitude of the Hankel functions, the MLFMM suffers a low frequency breakdown. This makes the numerical evaluation of the MLFMM diagonal plane wave based translation operators very difficult [2]. Hence, other approaches have to be found. One possibility to overcome this drawback is to include evanescent waves within the respective translation operators to better capture reactive fields [3]. Furthermore, it is also possible to work with the standard multipole-based translation operators at low frequencies [4], which are full operators. With respect to the diagonal MLFMM, both approaches have increased computational complexity.

For approximating smoother fields at lower frequencies, polynomial field representations appear to be very appropriate as low interpolation orders may be sufficient. One popular method working with a non-hierarchical approximation on a grid of equally spaced points covering all objects is the adaptive integral method (AIM) [7]. Although the approximation itself is non-hierarchical, a hierarchical acceleration of the translation step is performed by an FFT. Due to the AIM grid structure, empty portions of the solution domain are also covered causing unnecessary computations.

A hierarchical method employing multilevel Taylor series expansion of the respective Green's functions is presented in [5]. In [6], a method based on Lagrange interpolation of the Green's functions is proposed. The advantage of Lagrange interpolation is its rather constant approximation

error throughout the interpolation domain due to several interpolation points, whereas the approximation error of the Taylor expansion increases with distance from the single expansion point.

In this contribution, a method working with multilevel Lagrange interpolation based polynomial factorization of Green's functions, which is fully compatible with the well-known MLFMM oct-tree is presented. Firstly introduced in [8] for perfectly electric conducting (PEC) objects and mixed-potential electric field integral equation (MPIE) formulation, the method has been expanded for the treatment of IBC objects. The method is also applied to magnetic field integral equation (MFIE). Mixed-potential and dyadic integral equation formulations for electric and magnetic currents are considered and compared. The translations are only performed between non-empty boxes within the multilevel configuration. On the various levels, translations are accelerated by FFT without loss of accuracy. Due to the involved oct-tree structure, near-couplings can be computed by direct-MoM. Hence, no pre-correction step is necessary as in AIM or other pre-corrected FFT methods. The excellent performance of the algorithm, especially for low-frequency applications, is demonstrated in several examples.

II. INTEGRAL EQUATION FORMULATION

Consider a time-harmonic (time dependence $e^{j\omega t}$ suppressed) discretized surface integral equation (IE)

$$[Z_J]\{J\} + [Z_M]\{M\} = \{e\}. \quad (1)$$

$\{J\}$ and $\{M\}$ are the unknown electric and magnetic surface current expansion coefficient vectors and $\{e\}$ is the excitation vector due to an incident plane wave or a delta-gap source [1, 2]. Rao-Wilton-Glisson (RWG) vector basis functions $\mathbf{b}_n(\mathbf{r}')$ and either RWG or $\hat{\mathbf{n}} \times \text{RWG}$ testing functions $\mathbf{a}_m(\mathbf{r}) = \hat{\mathbf{n}} \times \mathbf{b}_m(\mathbf{r})$, $\hat{\mathbf{n}}$ being the respective surface normal vector, are employed.

The respective MoM matrix entries are given by

$$\begin{aligned} Z_{mn,J}^{direct} = & -j\omega\mu\alpha \langle \mathbf{b}_m(\mathbf{r}), \mathbf{L}(\mathbf{b}_n(\mathbf{r}')) \rangle \\ & + \frac{Z}{2}(1-\alpha) \left[\langle \mathbf{a}_m(\mathbf{r}), \mathbf{a}_n(\mathbf{r}') \rangle \right. \\ & \left. + 2 \langle \mathbf{a}_m(\mathbf{r}), \mathbf{K}(\mathbf{b}_n(\mathbf{r}')) \rangle \right], \end{aligned} \quad (2)$$

$$\begin{aligned} Z_{mn,M}^{direct} = & -\frac{\alpha}{2} \left[\langle \mathbf{b}_m(\mathbf{r}), \mathbf{a}_n(\mathbf{r}') \rangle \right. \\ & \left. + 2 \langle \mathbf{b}_m(\mathbf{r}), \mathbf{K}(\mathbf{b}_n(\mathbf{r}')) \rangle \right] \\ & - j\omega Z \varepsilon (1-\alpha) \langle \mathbf{a}_m(\mathbf{r}), \mathbf{L}(\mathbf{b}_n(\mathbf{r}')) \rangle, \end{aligned} \quad (3)$$

with the inner product

$$\langle \mathbf{v}(\mathbf{r}), \mathbf{w}(\mathbf{r}) \rangle = \iint_A \mathbf{v}(\mathbf{r}) \cdot \mathbf{w}(\mathbf{r}) da \quad (4)$$

and the operators

$$\begin{aligned} \mathbf{L}(\mathbf{v}(\mathbf{r}')) &= \iint_{A'} \bar{\mathbf{G}}(\mathbf{r}, \mathbf{r}') \cdot \mathbf{v}(\mathbf{r}') \\ \mathbf{K}(\mathbf{v}(\mathbf{r}')) &= \iint_{A'} \nabla G(\mathbf{r}, \mathbf{r}') \times \mathbf{v}(\mathbf{r}'). \end{aligned} \quad (5)$$

The excitation vector elements are

$$\begin{aligned} e_m(\mathbf{r}) = & -\iint_A \left\{ \mathbf{b}_m(\mathbf{r}) \cdot \alpha \left[\mathbf{E}^{inc}(\mathbf{r}) \right. \right. \\ & \left. \left. + Z(1-\alpha)(\hat{\mathbf{n}} \times \mathbf{H}^{inc}(\mathbf{r})) \right] \right\} da. \end{aligned} \quad (6)$$

The parameters μ , ε , k and $Z = \sqrt{\mu/\varepsilon}$ are the permeability, permittivity, wavenumber and wave impedance of free-space. $G(\mathbf{r}, \mathbf{r}') = e^{-jk|\mathbf{r}-\mathbf{r}'|}/(4\pi|\mathbf{r}-\mathbf{r}'|)$ is the homogeneous space scalar Green's function, $\bar{\mathbf{G}}(\mathbf{r}, \mathbf{r}') = (\bar{\mathbf{I}} + \mathbf{1}/k^2 \nabla \nabla)G(\mathbf{r}, \mathbf{r}')$ the electric field dyadic Green's function, and α the so-called combined field integral equation (CFIE) combination parameter with $0 \leq \alpha \leq 1$. $\mathbf{E}^{inc}(\mathbf{r})$ and $\mathbf{H}^{inc}(\mathbf{r})$ are the electric and magnetic field strength due to the respective excitation.

No magnetic surface currents \mathbf{M}_A with the expansion coefficients $\{M\}$ occur at the respective Huygens' surface if a PEC object is analyzed and equations (1) and (2) determine a unique solution for $\{J\}$. However, in general this set of equations is under-determined and additional equations are required. For this purpose, the common impedance boundary condition [10] is utilized for dielectrically coated PEC objects. The IBC is defined on the boundary between the exterior of the coating and the surrounding medium. It is formulated as

$$\mathbf{M}_A = Z_A (\mathbf{J}_A \times \hat{\mathbf{n}}). \quad (7)$$

Z_A is the characteristic surface impedance which can be approximated according to [10] as $Z_A \approx jZ\sqrt{\mu_r/\varepsilon_r} \tan(kd\sqrt{\mu_r\varepsilon_r})$ with the relative permeability and permittivity μ_r and ε_r and the thickness d of the coating. The IBC (7) is then

discretized according to [11] and the resulting equations are directly considered within an iterative solver.

The hyper-singular integrals in (2) and (3) can be avoided by the so-called mixed-potential formulation which has only weak $\mathbf{1}/R$ -singularities with $R = |\mathbf{r} - \mathbf{r}'|$. After applying some vector-analytic manipulations to (2) and (3), especially the surface divergence theorem [1], the inner products involving $\nabla \nabla G(\mathbf{r}, \mathbf{r}')$ are rewritten in the following manner [11]:

$$\langle \mathbf{a}(\mathbf{r}), \mathbf{L}_{\nabla \nabla}(\mathbf{b}(\mathbf{r}')) \rangle = \oint_{C_m} \mathbf{a}(\mathbf{r}) \cdot \hat{\mathbf{u}}_m L_s(\nabla \cdot \mathbf{b}(\mathbf{r}')) dC_m \quad (8)$$

$$\langle \mathbf{b}(\mathbf{r}), \mathbf{L}_{\nabla \nabla}(\mathbf{b}(\mathbf{r}')) \rangle = \langle \nabla \cdot \mathbf{b}(\mathbf{r}), L_s(\nabla \cdot \mathbf{b}(\mathbf{r}')) \rangle,$$

with the operators

$$\begin{aligned} \mathbf{L}_{\nabla \nabla}(\mathbf{v}(\mathbf{r}')) &= \iint_{A'} \nabla \nabla G(\mathbf{r}, \mathbf{r}') \cdot \mathbf{b}(\mathbf{r}') da' \\ L_s(s(\mathbf{r}')) &= \iint_{A'} G(\mathbf{r}, \mathbf{r}') s(\mathbf{r}') da'. \end{aligned} \quad (9)$$

C_m is the boundary curve of the test domain and $\hat{\mathbf{u}}_m$ is the unit vector in the tangent plane and perpendicular to C_m . The mixed-potential coupling integrals with (8) and (9) applied to (2) and (3), respectively, are named $\mathbf{Z}_{mn,J}^{mixed}$ and $\mathbf{Z}_{mn,M}^{mixed}$ in the following.

For reducing redundancy of the discretized IE operators, which are in general fully-populated with respect to the contained far-interactions, an appropriate basis change is performed for these far-interactions. The basis change is achieved by multilevel Lagrange interpolation of the pertinent Green's functions, where the current basis functions are mapped on the interpolation samples. A further speed-up is reached by FFT acceleration for the computation of the multilevel interactions among the interpolation samples.

III. LAGRANGE INTERPOLATION OF GREEN'S FUNCTIONS

The electric field dyadic Green's function $\bar{\mathbf{G}}(\mathbf{r}, \mathbf{r}')$, the scalar Green's function $G(\mathbf{r}, \mathbf{r}')$ and its gradient $\nabla G(\mathbf{r}, \mathbf{r}')$ can be factorized by Lagrange interpolation with respect to \mathbf{r} and \mathbf{r}' employing Lagrange interpolation factors according to

$$\begin{aligned} \tilde{\bar{\mathbf{G}}}(\mathbf{r}, \mathbf{r}') &= \sum_{i=1}^{N_p^3} \sum_{j=1}^{N_p^3} \Lambda_i(\mathbf{r}) \Lambda_j(\mathbf{r}') \tilde{\bar{\mathbf{G}}}_{ij}(\mathbf{r}_i, \mathbf{r}'_j) \\ \tilde{G}(\mathbf{r}, \mathbf{r}') &= \sum_{i=1}^{N_p^3} \sum_{j=1}^{N_p^3} \Lambda_i(\mathbf{r}) \Lambda_j(\mathbf{r}') G_{ij}(\mathbf{r}_i, \mathbf{r}'_j) \\ \tilde{(\nabla G)}(\mathbf{r}, \mathbf{r}') &= \sum_{i=1}^{N_p^3} \sum_{j=1}^{N_p^3} \Lambda_i(\mathbf{r}) \Lambda_j(\mathbf{r}') \nabla G_{ij}(\mathbf{r}_i, \mathbf{r}'_j), \end{aligned} \quad (10)$$

with $\Lambda_i(\mathbf{r})$ being the respective Lagrange polynomials and N_p the number of interpolation points. When inserted in equations (2) and (3), the resulting integrals can be pre-computed and do not have to be evaluated in every matrix-vector product within an iterative solver.

By this Lagrange interpolation point representation, an accelerated evaluation of the discretized IE operators can be achieved in two ways. First, the necessary number of interpolation points can be considerably smaller than the number of basis functions. This is in particular the case for low-frequency applications where very many discretization steps per wavelength are needed in order to represent fine geometrical details. Second, the coupling computation effort can be considerably reduced when employing an FFT-based coupling computation.

IV. DIAGONALIZATION OF THE TRANSLATION OPERATOR

The computational effort of the presented Lagrange interpolation based integral equation representation has a disadvantageous large computational effort for the far-interactions of $O(N_p^3 N_p^3) = O(N_p^6)$ for one pair of interpolation domains (3D cubes) with N_p being the number of interpolation points. This is because the interpolations must in general be performed in three dimensions, even if a surface integral equation is considered. Furthermore, the corresponding translation operators are still full operators.

To overcome this drawback, an FFT-based method for diagonalizing the corresponding translation operators is employed. In particular the formulation for $\mathbf{Z}_{mn,J}^{direct}$ according to (1) and (2) is considered but everything applies in similar form also for $\mathbf{Z}_{mn,J}^{mixed}$ and all other matrices. The approximated matrix $\tilde{\mathbf{Z}}_{mn,J}$ with the interpolated dyadic Green's function according to (10) can be formulated as

$$\begin{aligned} \tilde{Z}_{mn,J} = & \sum_{i=1}^{N_p^3} \iint_A \Lambda_i(\mathbf{r}) \mathbf{b}_m(\mathbf{r}) da \\ & \cdot \sum_{i'=1}^{N_p^3} \bar{\mathbf{G}}(\mathbf{r}_i, \mathbf{r}_{j'}) \cdot \iint_{A'} \Lambda_{i'}(\mathbf{r}') \mathbf{b}_n(\mathbf{r}') da'. \end{aligned} \quad (11)$$

As it can be seen, the Green's function is factorized by the Lagrange interpolation with respect to \mathbf{r} and \mathbf{r}' so that the integrals in (11) can be pre-computed.

Employing tensor notation with third order tensors, each order corresponding to one Cartesian dimension, the j summation in (11) can be rewritten as

$$[\mathbf{R}]_{ix,iy,iz}^3 = \sum_{ix'=1}^{N_p} \sum_{iy'=1}^{N_p} \sum_{iz'=1}^{N_p} \bar{\mathbf{G}}(\Delta i_x, \Delta i_y, \Delta i_z) \cdot [\mathbf{S}]_{ix',iy',iz'}^3, \quad (12)$$

with the third order tensors $[\mathbf{S}]^3$ and $[\mathbf{R}]^3$ containing the source or receive integrals, respectively, and $\Delta i_k = i_k - i'_k$. This discrete convolution in space domain with equidistant sampling can efficiently be computed in spectral domain according to

$$\begin{aligned} [\mathbf{R}]_{ix,iy,iz}^3 &= \sum_{ix'=1}^{2N_p-1} \sum_{iy'=1}^{2N_p-1} \sum_{iz'=1}^{2N_p-1} [\bar{\mathbf{G}}]_{\Delta(i_x,i_y,i_z)}^3 \cdot [\mathbf{S}]_{ix',iy',iz'}^3 \\ &= F^{-1} \left\{ F \left\{ [\bar{\mathbf{G}}]^3 \right\} \otimes F \left\{ [\mathbf{S}]^3 \right\} \right\}. \end{aligned} \quad (13)$$

Zero-padding has to be performed in order to avoid aliasing errors. The symbol " \otimes " denotes the Hadamard (tensor element-wise) dyadic-vector product in the discrete Fourier domain. It is essential, that the necessary forward transformations F and backward transformations F^{-1} are performed by FFT to obtain enhanced computational efficiency when employing (13) instead of (11). In the end, the receive contributions in $[\mathbf{R}]^3$ must be multiplied with the test integrals. Since the translations are computed as Hadamard products in the discrete Fourier domain, diagonalization of the translation operators has been achieved. However, the computational complexity is then dominated by the transformations instead of the coupling computations itself. Together with the necessary zero-padding, the overall procedure appears to be efficient only for relatively large numbers of interpolation points, as e.g. obtained if the whole radiation or scattering object is covered with one regular grid.

By numerical experiments it was found that employing (13) is advantageous even for the small

number of 3 interpolation points per Cartesian dimension. For cubic interpolation with $N_p = 4$, which is mostly a good choice for accurate computations, there is a reduction in translation time by a factor of about 7. Due to this observation, FFT-based translations are employed within this fast solver. The complexity of the translation is $O(N_p^3 \log N_p^3) = O(N_p^3 \log N_p)$ with respect to the number of interpolation points N_p instead of $O(N_p^6)$ for direct translation in space domain.

VI. MULTILEVEL ALGORITHM

One major drawback of grid based fast solvers is the general necessity to work with 3 dimensional grids although the problem itself is a 2 dimensional surface problem. Especially dominant is this drawback in AIM or pre-corrected FFT techniques. There, all coupling computations are performed by a global 3D FFT on a single grid covering the whole computation domain. Hence, most computations are performed for grid points located in the empty space inside the computation domain. To relieve this problem, a multilevel algorithm following a hierarchical oct-tree grouping strategy is developed, where regular grids within the individual groups are considered and where the translations among non-empty groups are computed by employing FFT-acceleration.

A cubic oct-tree structure as known from the MLFMM algorithm [2] is assumed. The distances d between different box centers on a given level lev are found to be

$$\begin{aligned} d_{lev}^{near} &= n_1 a_{lev} \\ d_{lev}^{far} &= n_2 a_{lev}. \end{aligned} \quad (14)$$

d_{lev}^{near} is the near-coupling range for each level lev , where the necessary interactions are computed on finer levels or by direct MoM integration. d_{lev}^{far} is the far-coupling range up to which far translations are performed on the corresponding level and a_{lev} is the edge length of each cube in the pertinent level. On all levels, the relation $a_{lev+1} = 2 a_{lev}$ is valid.

The described Lagrange interpolation algorithm with FFT acceleration is employed for boxes with separations $d_{lev}^{near} \leq d \leq d_{lev}^{far}$. Interactions among boxes with $d > d_{lev}^{far}$ are computed on the next coarser level $lev + 1$. For levels with a small box-size as compared to wavelength, the number

of interpolation points per dimension N_p^{lev} on a certain level lev can be kept constant on different levels as suggested in [12]. As the resulting impedance matrix is then an \mathbf{H}^2 -matrix [12], computational and storage complexity per matrix-vector product are $O(N)$. This strategy is only valid for fine levels with box sizes significantly smaller than the wavelength. Hence, we use this strategy if a_{lev+1}/λ is below a constant threshold r^{const} . Following this strategy, a coarser level source tensor $[\mathbf{S}^{lev+1}]^3$ is Lagrange antepolated for aggregation case

$$[\mathbf{S}^{lev+1}]_{ix',iy',iz'}^3 = \sum_{i_x=1}^{N_p} \sum_{i_y=1}^{N_p} \sum_{i_z=1}^{N_p} \Lambda_{ix,iy,iz,ix',iy',iz'} [\mathbf{S}^{lev}]_{ix,iy,iz}^3, \quad (15)$$

where the interpolation points on all levels are equally spaced in each dimension in order to realize a regular grid. The disaggregation procedure is performed in the same manner by interpolating finer level receive contributions from corresponding coarser level receive contributions. All aggregation factors can be pre-computed before evaluating the matrix-vector product. Due to the orthogonality of the Lagrange polynomials, the operators contain a lot of zero entries, which leads to computation time and memory reduction.

If the box size is not small compared to the wavelength, the absolute interpolation point distance is maintained on coarser levels. No Lagrange interpolation is necessary as all coarser level points are at the same position as at least one finer level interpolation point and the accordant Lagrange polynomials are orthogonal. Hence, (15) reduces to

$$[\mathbf{S}^{lev+1}]_{ix+\Delta ix,y+\Delta iy,z+\Delta iz}^3 = [\mathbf{S}^{lev}]_{ix,iy,iz}^3, \quad (16)$$

for the aggregation case, whereas $N_p^{lev} = N_p$ at the finest level following this strategy and $N_p^{lev+1} = 2N_p^{lev} - 1$ for all subsequent coarser levels. Δix , Δiy , and Δiz are index offsets dependent on the position of the finer level group within the coarser level group.

For disaggregation case, the pertinent receive contributions from the coarser level have just to be copied on the finer level. Following this strategy, the computational complexity increases as the required number of interpolation points roughly doubles in each direction. The computational complexity following this strategy is

$O(N^{3/2} \log(N))$ in conjunction with FFT-based translations and is thus significantly worse compared to fast high frequency solvers like MLFMM with $O(N \log(N))$ complexity. The proposed algorithm is thus especially suited for low-frequency problems where the fine-level strategy can be employed for most levels.

VI. Dyadic versus mixed-potential MLIPFFT

The presented multilevel interpolatory FFT accelerated method (MLIPFFT) is employed to direct field integral equations according to (2) and (3) as well as to the more common mixed potential integral equations (MPIE) according to (8)-(10). In a previous work [9] it has been shown, that the MPIE is preferable for interpolation in well-conditioned problems as the computation time per matrix-vector product is smaller than for the EFIE and MFIE with dyadic Green's function formulation. For ill-conditioned problems, the direct field EFIE and MFIE with dyadic Green's functions are preferable as the isolated electric scalar potential and the superposition of the potential contributions of the MPIE usually need a higher interpolation accuracy.

VII. NUMERICAL RESULTS

The efficiency of the presented algorithm is shown for several computation examples. All computations shown in this section have been carried out on one core of a Dell Precision T7500 workstation (2.53 GHz clock speed, 96 GByte RAM).

As a linear equation system solver, a flexible generalized minimal residual solver with Given's rotations was used. As an iteration stop criterion, a residual error of 10^{-4} was configured.

A. Sphere with dielectric coating

A PEC sphere with diameter 1 m and a dielectric coating of 2.5 cm thickness ($\epsilon_r = 4 - j100$) is computed as a first example. It is discretized by 176 472 unknowns (88 236 electric and magnetic current unknowns, respectively). The object is illuminated by a plane wave with a frequency of 500 MHz. In Fig. 1a, the bistatic radar cross section (RCS) of the sphere is depicted for an MLIPFFT computation employing the IBC (direct field formulation) compared to an analytical Mie

series solution. As can be seen, both results show excellent agreement. Figure 1b shows the object and the resulting magnetic current distribution. For the MLIPFFT, the total solution time was 2 171 sec with a memory consumption of 1 522 MByte.

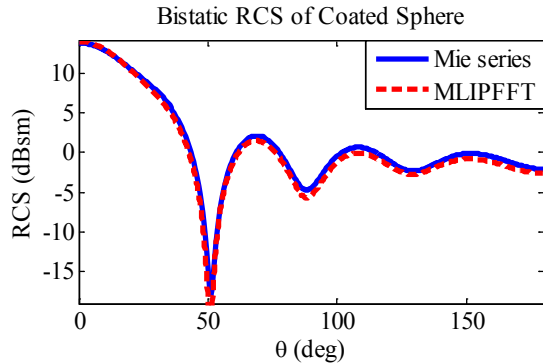


Fig. 1a. Bistatic RCS of a sphere with dielectric coating.

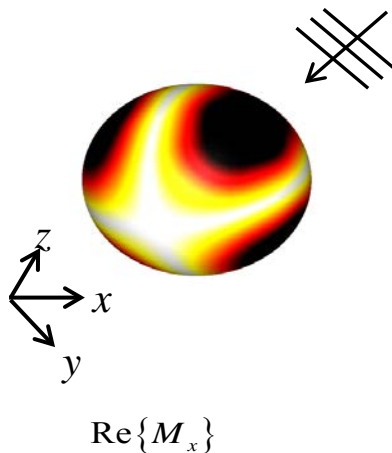


Fig. 1b. x -component of magnetic current distribution on dielectric sphere (real part).

B. Parabolic reflector

The second example is a 3λ PEC parabolic reflector, which is vertically illuminated by a plane wave. The reflector is densely discretized resulting in 222 583 unknowns. The MLIPFFT computation employing a mixed-potential EFIE was performed within 5 577 sec and with a total memory consumption of 1 873 MByte. For comparison, the computation was also performed by an MLFMM within 9 066 sec and with 9 475 MByte memory consumption. Both RCS results are shown in Fig. 2a and the accordant current distribution in Fig. 2b.

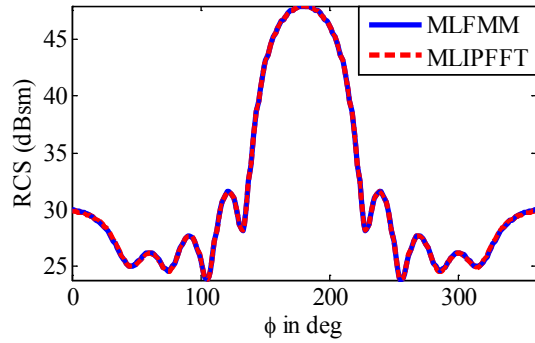


Fig. 2a. Bistatic $\theta\phi$ -RCS of a parabolic reflector.

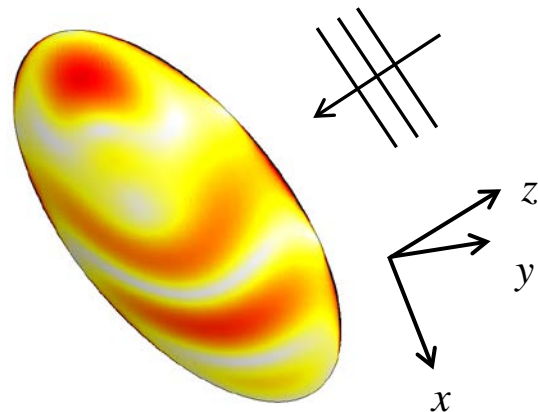


Fig. 2b. Electric current distribution on parabolic reflector (real part).

C. P3-Orion

The last example is the flight object ‘‘P3-Orion’’ with a length of 35 m. At first, the object’s surface material is PEC. The object is discretized with 536 250 electric current unknowns and illuminated by a plane wave incident from $\theta_i = 90^\circ, \phi_i = 20^\circ$ with a wavelength of 36 m. The accordant MLIPFFT computation time was 12 675 sec and the required memory 7 718 MByte. Second, the problem was computed for a finite conducting coating ($\sigma = 10^{-1}$ S/m) of the object employing IBC. The computation time was 18 793 sec and the memory demand 13 610 MByte. The accordant bistatic $\phi\theta$ -RCS results are depicted in Fig. 3a. Figure 3b shows the object and the electric current distribution.

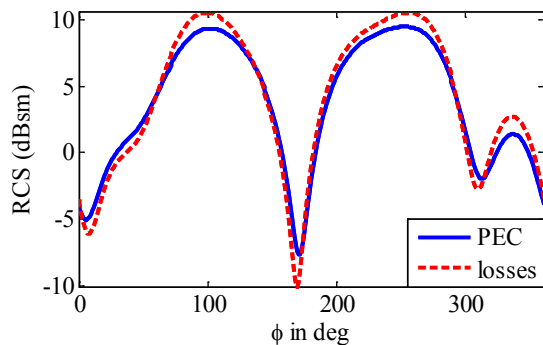


Fig. 3a. Bistatic RCS of P3-Orion.

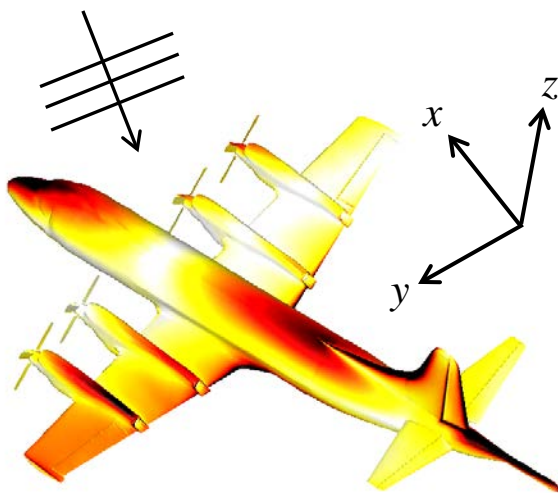


Fig. 3b. Electric current distribution on P3-Orion.

VIII. CONCLUSIONS

A fast integral equation fast solver, which is especially suited for low frequencies, has been presented. By 3D FFT, the accordant translation operators are diagonalized. Even for small numbers of interpolation points, this FFT-based technique has shown to be effective. Furthermore, an oct-tree based adaptive multilevel scheme reduces the computation of empty space and makes the algorithm useful for broadband applications and combinable with a high-frequency fast solver. The interpolation-based fast solver has demonstrated excellent efficiency and accuracy for PEC and impedance boundary body problems.

REFERENCES

- [1] S. M. Rao, D. R. Wilton, and A. W. Glisson, "Electromagnetic Scattering by Surfaces of Arbitrary Shape", *IEEE Trans. Antennas Propagat.*, vol. 30, no. 3, pp. 409–418, May 1982.
- [2] W. C. Chew, J. Jin, E. Michielssen, and J. Song, *Fast and Efficient Algorithms in Computational Electromagnetics*, Boston, MA: Artech House, 2001.
- [3] D. Wulf and R. Bunger, "An Efficient Implementation of the Combined Wideband MLFMA/LF-FIPWA," *IEEE Trans. Antennas Propagat.*, vol. 57, no. 12, pp. 467–474, Feb 2009.
- [4] L. J. Jiang and W. C. Chew, "A Mixed-Form Fast Multipole Algorithm," *IEEE Trans. Antennas Propagat.*, vol. 53, no. 12, pp. 4145–4156, Dec. 2005.
- [5] M. Vikram, H. Huang, B. Shanker, and T. Van, "A Novel Wideband FMM for Fast Integral Equation Solution of Multiscale Problems in Electromagnetics," *IEEE Trans. Antennas Propagat.*, vol. 57, no. 7, pp. 2094–2104, July 2009.
- [6] H. Wang and C. Chan, "The Implementation of Multilevel Green's Function Interpolation Method for Full-Wave Electromagnetic Problems," *IEEE Trans. Antennas Propagat.*, vol. 55, no. 5, pp. 1348–1358, May 2007.
- [7] E. Bleszynski, M. Bleszynski, and T. Jaroszewicz, "AIM: Adaptive Integral Method for Solving Large-Scale Electromagnetic Scattering and Radiation Problems," *Radio Sci.*, vol. 31, pp. 1225–1251, 1996.
- [8] D. Schobert and T. Eibert, "A Multilevel Interpolating Fast Integral Solver with Fast Fourier Transform Acceleration," *URSI EMTS*, pp. 539–542, 2010.
- [9] D. T. Schobert, T. F. Eibert, and C. H. Schmidt, "Fast Fourier Transform Accelerated Multilevel Green's Function Interpolation for Mixed Potential and Direct Field Surface Integral Equations," *EU-CAP Conference*, pp. 3208–3211, 2011.
- [10] J. Jin, *The Finite Element Method in Electromagnetics*, New York: John Wiley & Sons, 2002.
- [11] Ismatullah and T. F. Eibert, "Surface Integral Equation Solutions by Hierarchical Vector Basis Functions and Spherical Harmonics Based Multilevel Fast Multipole Method," *IEEE Trans. Antennas Propagat.*, vol. 57, no. 7, pp. 2084–2093, July 2009.
- [12] W. Hackbusch and S. Boerm, " H^2 –Matrix Approximation of Integral Operators by Interpolation," *Applied Numerical Mathematics*, vol. 43, no. 1-2, pp. 129–143, 2002.
- [13] M. Li, H. Chen, C. Li, R. Chen, and C. Ong, "Hybrid UV/MLFMA Analysis of Scattering by PEC Targets above a Lossy Half-Space," *Applied*

Computational Electromagnetic Society (ACES) Journal, vol. 26, no. 1, pp. 17–25, January 2011.

- [14] S. Seo, C. Wang, and J. Lee, “Analyzing PEC Scattering Structure Using an IE-FFT Algorithm,” *Applied Computational Electromagnetic Society (ACES) Journal*, vol. 24, no. 2, pp. 116–128, April 2009.
- [15] C. Luo and C. Lu, “Electromagnetic Scattering Computation Using a Hybrid Surface and Volume Integral Equation Formulation,” *Applied Computational Electromagnetic Society (ACES) Journal*, vol. 22, no. 3, pp. 340–349, November 2007.
- [16] X. Xu, Q. Liu, and Z. Zhang, “The Stabilized Biconjugate Gradient Fast Fourier Transform Method for Electromagnetic Scattering,” *Applied Computational Electromagnetic Society (ACES) Journal*, vol. 17, no. 1, pp. 97–103, March 2002.



Dennis T. Schobert received his Dipl.-Ing. (M.Sc.) degree in Electrical Engineering from Technische Universität Dresden, Dresden, Germany, in 2009. Since 2009, he is with the Lehrstuhl für Hochfrequenztechnik at Technische Universität München, Munich, Germany as a research

assistant. His major research interests include fast integral equation solvers and novel automotive communication techniques.



Thomas F. Eibert received the Dipl.-Ing. (FH) degree from Fachhochschule Nürnberg, Nürnberg, Germany, the Dipl.-Ing. degree from Ruhr-Universität Bochum, Bochum, Germany, and the Dr.-Ing. degree from Bergische Universität Wuppertal, Wuppertal, Germany, in 1989, 1992, and 1997, all in Electrical Engineering. From 1997 to 1998, he was with the Radiation Laboratory, EECS Department of the University of Michigan, Ann Arbor, MI, USA from 1998 to 2002, he was with Deutsche Telekom, Darmstadt, Germany, and from 2002 to 2005, he was with the Institute for High-frequency Physics and Radar Techniques of FGAN e.V., Wachtberg, Germany, where he was head of the department Antennas and Scattering. From 2005 to 2008, he was a Professor for radio frequency technology at Universität Stuttgart, Stuttgart, Germany.

Since October 2008, he has been a Professor for high-frequency engineering at the Technische Universität München, Munich, Germany. His major areas of interest are numerical electromagnetics, wave propagation, measurement techniques for antennas and scattering as well as all kinds of antenna and microwave circuit technologies for sensors and communications.